J. Fluid Mech. (1995), *vol.* 294, *pp.* 47–69

The dynamics of driven rotating flow in stadium-shaped domains

By J. J. KOBINE[1], T. MULLIN[1] AND T. J. PRICE[2]

[1]Atmospheric Physics, Department of Physics, Clarendon Laboratory, University of Oxford, Parks Road, Oxford, OX1 3PU, UK

[2]Laboratoire de Physique Statistique, Ecole Normale Supérieure, 24 rue Lhomond, 75231 Paris Cedex 05, France

(Received 11 July 1994 and in revised form 1 March 1995)

Results are presented from an experimental investigation of the dynamics of driven rotating flows in stadium-shaped domains. The work was motivated by questions concerning the typicality of low-dimensional dynamical phenomena which are found in Taylor–Couette flow between rotating circular cylinders. In such a system, there is continuous azimuthal symmetry and travelling-wave solutions are found. In the present study, this symmetry is broken by replacing the stationary outer circular cylinder with one which has a stadium-shaped cross-section. Thus there is now only discrete symmetry in the azimuthal direction, and travelling waves are no longer observed. To begin with, the two-dimensional flow field was investigated using numerical techniques. This was followed by an experimental study of the dynamics of flow in systems with finite vertical extent. Configurations involving both right-circular and tapered inner cylinders were considered. Dynamics were observed which correspond to known mechanisms from the theory of finite-dimensional dynamical systems. However, flow behaviour was also observed which cannot be classified in this way. Thus it is concluded that while certain low-dimensional dynamical phenomena do persist with breaking of the continuous azimuthal symmetry embodied in the Taylor–Couette system, sufficient reduction of symmetry admits behaviour at moderately low Reynolds number which is without any low-dimensional characteristics.

1. Introduction

A typical experience in the study of fluid dynamics is that increasing the Reynolds number for a given flow field leads to a change from regular to irregular behaviour. Much attention has been directed towards those fluid systems which go through a definite sequence of instabilities in this respect, since it is often possible to analyse such problems using hydrodynamic stability theory, while at the same time carrying out careful experimental investigations. The success of these two approaches in combination is reflected in our understanding of problems such as Rayleigh–Bénard convection (Libchaber & Maurer 1980; Gollub & Benson 1980) or Taylor–Couette flow (Di Prima & Swinney 1981; Mullin 1993*a*). However, it is interesting to ask just how typical this well-defined behaviour is. It is not unreasonable to suppose that it may be special to closed flows, as opposed to open flows such as boundary layers or wakes. In the case of Taylor–Couette flow in particular, the sense of atypicality is heightened by the existence of cells and travelling waves which persist to very high Reynolds numbers (Smith & Townsend 1982).

The present study is an attempt to establish the typicality or otherwise of occurrences of low-dimensional behaviour in closed recirculating flows between concentric cylinders. The most familiar problem in this class is Taylor–Couette flow between concentric circular cylinders. This system is characterized by continuous $SO(2)$ symmetry in the azimuthal direction which supports travelling waves that propagate around the annulus. However, if this non-generic symmetry is broken, then travelling-wave solutions are prohibited. An approach which has been adopted in previous investigations (Snyder 1968; Mullin, Lorenzen & Pfister 1983; Mullin & Lorenzen 1985; Kobine & Mullin 1994) is to change the shape of the stationary outer cylinder, thereby affecting the azimuthal symmetry of the domain in which flow occurs. It has been the purpose of recent studies, including the present one, to determine whether or not the low-dimensional bifurcation phenomena which are observed in the standard system (see Mullin 1993*a*, for example) are structurally stable to this breaking of the continuous azimuthal symmetry.

The role played by azimuthal symmetry in deciding the form of steady flows appears to have been considered first by Terada & Hattori (1926). They performed a series of experiments in which flow was driven between a stationary circular outer cylinder and a variety of rotating inner devices. These included a concentric circular cylinder with a stationary barrier across the gap, an eccentric circular cylinder and finally a pair of circular cylinders. In all these cases the continuous azimuthal symmetry of the standard problem was broken by the change in geometry. Nevertheless, steady cellular flows similar to Taylor-vortex flow were observed in each case for sufficient angular speed of the rotating element.

A symmetry variant which has been studied extensively in more recent years has the outer circular cylinder replaced by one with square cross-section, while retaining the circular inner cylinder. The azimuthal symmetry of the flow domain is now that of the discrete Z_4 group. Such a system was first considered by Snyder (1968), who showed experimentally that there is a transition from featureless flow to steady cellular flow with increase of the speed of the inner cylinder. This cellular flow is equivalent to Taylor-vortex flow, although the cells are no longer axisymmetric. The solution structure of steady flows in this square system was investigated experimentally by Mullin & Lorenzen (1985) and Kobine & Mullin (1994). It was found that apart from minor differences the steady flows exhibit a bifurcation structure which is qualitatively the same as the one which is now well understood in Taylor–Couette flow. In addition, dynamic flow phenomena in the single-cell flow in the square system were studied by Kobine & Mullin (1994). A complicated but self-consistent solution structure was uncovered, consisting entirely of behaviour which can be described in the context of finite-dimensional dynamical systems. Central to this was the observation of a time-dependent motion which, when analysed as trajectories in a reconstructed phase space, suggests dynamics of the type proposed by Šil'nikov (1965) involving an orbit which is homoclinic to a saddle-focus. Similar dynamics have been observed by Mullin & Price (1989) in a Taylor–Couette system with $SO(2)$ azimuthal symmetry.

In this paper, we make a further reduction in the azimuthal symmetry by using as the outer cylinder a container whose cross-section is that of a stadium. The geometry is illustrated in figure 1(*a*). There are two parallel sides and two semicircular ends to the stadium, with a rotating cylinder situated inside. Thus there is now only discrete Z_2 symmetry azimuthally. Two different types of inner cylinder were used in the study. The first was a right-circular cylinder, giving rise to mirror symmetry about the horizontal midplane of the domain (figure 1*b*). The second type was a linearly tapered circular cylinder, leading to an asymmetric domain in the vertical direction

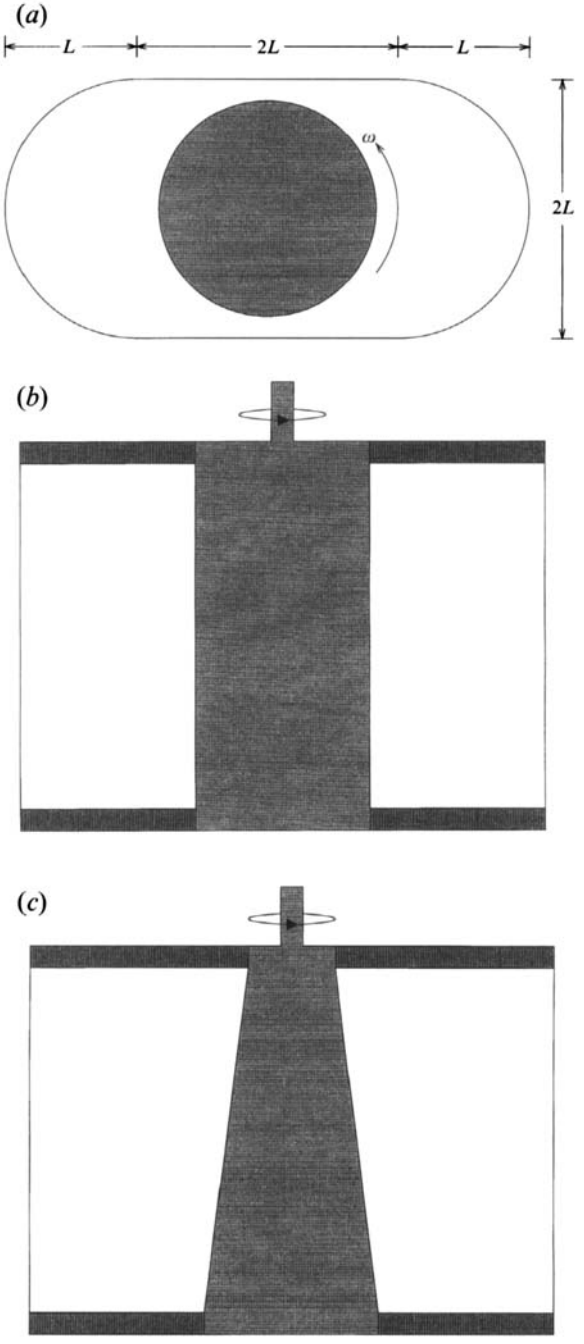

FIGURE 1. Geometry of the stadium-shaped Taylor–Couette system: (*a*) plan view; (*b*) front view of system with right-circular cylinder; (*c*) front view of system with tapered inner cylinder.

(figure 1*c*). The motivation for studying the flow in these stadium systems was that, by systematically reducing the symmetry to such an extent compared with the symmetries of the original and the square Taylor–Couette problems, it might be impossible for the flow dynamics to be described by simple low-dimensional mechanisms. If, on the

other hand, finite-dimensional behaviour could be observed, then it would support the findings of previous research which point to such behaviour being structurally stable to breaking of the $SO(2)$ symmetry.

We begin by considering in §2 the nature of the steady two-dimensional flow which is driven by a rotating right-circular cylinder inside a stationary stadium. The streamlines for this flow have been calculated using a truncated series solution of the equations for creeping flow. Then in §3 there is a description of the experimental apparatus and methods which were used for this study. The results which were obtained for time-dependent flows driven by a right-circular inner cylinder are presented in §4. The flows that were driven by the tapered rotating cylinder are considered in §5. Finally, we present conclusions in §6 based on the findings of this work.

2. Structure of two-dimensional rotating flow in a stadium

Studies of two-dimensional flows in systems that are geometrically similar to the present one have been carried out by Schumack, Schultz & Boyd (1992) and Hellou & Coutanceau (1992). Schumack *et al.* used a spectral element method to calculate the flow between a rotating circular cylinder and a container, similar to an ellipse, formed from two circular arcs. The two-dimensional flow consisted of approximately circular streamlines around the inner cylinder, with recirculation regions in both corner ends of the outer container. The problem tackled by Hellou & Coutanceau was that of two-dimensional flow driven by the rotation of a circular cylinder at the centre of a rectangular box. The solution was obtained analytically, using a truncated-series approach to the biharmonic equation, and confirmed experimentally, using flow visualization techniques. Both methods gave a flow field which comprised a main circular flow around the inner cylinder, with driven recirculations in the outer regions of the domain.

Thus it is reasonable to expect that the two-dimensional flow for a rotating cylinder inside a stadium-shaped cylinder should be qualitatively the same as the flows discussed above. Indeed, all these systems can be viewed as truncated representations of the problem considered by Moffatt (1964) of two-dimensional flow driven by a rotating cylinder situated between two infinitely long parallel plates. Moffatt showed analytically that such a flow should consist of a rapidly decaying sequence of driven recirculations extending away in both directions from the cylinder. However, the analytical techniques used by Moffatt are not appropriate for the present case. In order to establish the exact nature of the stadium flow, we have calculated the two-dimensional streamline pattern using standard numerical methods. These methods are discussed briefly below, along with the results which were obtained.

Our numerical technique is similar to that used by Hellou & Coutanceau (1992) in their calculation of two-dimensional flow driven by a rotating cylinder in a rectangular channel. It uses a least-squares method to fit a truncated series solution of the equations for creeping flow with the appropriate boundary conditions for the velocity. We begin by assuming that the inertia terms in the time-independent Navier–Stokes equations are negligible in comparison with the viscous terms. Thus we have a flow which is governed by the equations for creeping motion, namely

$$-\nabla p + \mu \nabla^2 \boldsymbol{u} = 0, \tag{1a}$$

$$\nabla \cdot \boldsymbol{u} = 0. \tag{1b}$$

We adopt a Cartesian coordinate system with the z-axis coincident with the axis

of rotation, and restrict attention to two-dimensional flow where $\boldsymbol{u} = (u, v, 0)$ and all terms involving the operator $\partial/\partial z$ vanish. Thus we may introduce a stream function $\psi(x, y)$ such that $u = \partial\psi/\partial y$ and $v = -\partial\psi/\partial x$. Applying the curl operator to both sides of (1*a*) and rewriting in terms of ψ leads to the familiar biharmonic equation

$$\nabla^4\psi = 0. \tag{2}$$

Thus the problem is essentially one of solving (2) with the appropriate boundary conditions. These are set by the no-slip condition which constrains the velocity to be zero everywhere on the stationary stadium and directed tangentially with constant magnitude on the rotating circular cylinder.

Following Prosnak (1987), we represent the problem in the complex plane $z = x+\mathrm{i}y$ and work with the complex conjugate variables $z, \bar{z}$. The biharmonic equation becomes

$$\frac{\partial^4\psi}{\partial^2 z \partial^2 \bar{z}} = 0, \tag{3}$$

and this is directly integrable to give

$$\psi = \bar{z}f(z) + z\bar{f}(\bar{z}) + g(z) + \bar{g}(\bar{z}), \tag{4}$$

where $f(z)$ and $g(z)$ are arbitrary holomorphic functions.

The functions $f(z)$ and $g(z)$ are then chosen so that the velocity boundary conditions are satisfied, subject to the restriction that the physical quantities of velocity, vorticity and pressure are single valued. For all but the most geometrically simple domains, the holomorphic functions contain an infinite number of terms, so in practice we truncate the series and perform a least-squares fit as first suggested by Bourot (1969) and recently applied by Hellou & Coutanceau (1992). The discrete symmetries of the stadium configuration allow us to work in the positive quadrant only, and we retain 96 terms of the holomorphic series.

One result of applying the above procedure to the present problem is the streamline plot shown in figure 2. This plot shows the right-hand half of the fluid domain (the other half is simply a reflection in $x = 0$), and it can be seen that the main and secondary flows found in elliptical and rectangular geometries are also present in this case. There is a main circulating flow around the inner cylinder, with recirculations to its left and right; our numerical studies indicate that these recirculations persist down to a cross-sectional length-to-breadth ratio of 1.2. The stream function values marked in figure 2 show that the recirculations are much weaker than the circulating flow, although they occupy a significant area within the flow domain.

Knowledge of the two-dimensional flow field is important since it forms the basis of the more complicated three-dimensional flow structures which necessarily exist in a domain with finite vertical extent. In particular, the streamline plot in figure 2 shows important features which are pertinent when choosing a measuring position from which dynamical information is to be obtained. Thus we choose to locate the measuring point in the shear layer between the inner and outer recirculations where contributions to the dynamics from both regions are more easily identified. Also, fluid elements in the shear layer close to the inner cylinder experience alternating conditions of deceleration and acceleration around the region due to the presence of the parallel sides and the recirculation regions. Information of this type proves essential in the interpretation of the experimental results of the study.

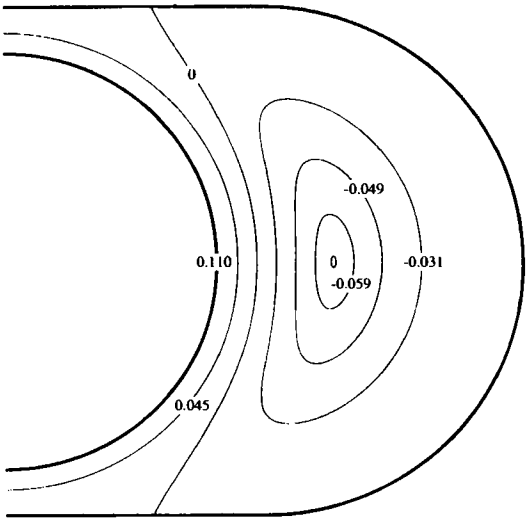

FIGURE 2. Streamlines for two-dimensional creeping flow driven by a rotating cylinder inside a stadium with $\eta = 0.824$. Only the right-hand half of the domain is shown; numbers indicate stream function values.

3. Experimental details

In this section, we discuss the apparatus and techniques which were used in the experimental investigation. Three different flow rigs are described, followed by details of the measurement process.

3.1. *Mechanical components*

The first flow rig which was constructed had a right-circular inner cylinder and a stadium-shaped outer cylinder. The sides of the outer container were flat Perspex plates, and the ends were formed from a 165 mm length of Perspex cylinder which was cut in half. These four pieces were glued together on a former to give the required stadium shape. The perpendicular distance between the two parallel sides, and the diameter of the semicircular ends, was equal to 107.6 ± 0.1 mm. The width of each of the two straight sides was equal to 109.8 ± 0.1 mm. Thus this rig had a cross-sectional length-to-breadth ratio of 2.02. The inner cylinder was made of brass, and had a diameter of 88.66 ± 0.01 mm. The stadium-shaped cylinder was set into a machined Perspex base, along with a circular PTFE bearing for the inner cylinder. The height of the flow domain was defined by the position of a horizontal PVC collar which fitted inside the stadium and around the right circular cylinder. This end-plate was supported from above by two metal rods which passed through the Perspex lid of the flow rig and were held by two screw grips. The working fluid was silicone oil with a kinematic viscosity $\nu = 16.9$ mm^{2}s^{-1} at 21.5°C.

A second flow rig was made to a very high tolerance in order to test the robustness of the results obtained with the apparatus described above. This stadium was made from two Perspex plates and the two halves of a 120 mm length of glass cylinder. The choice of glass as a material for the curved surfaces resulted in a more accurate radius than was the case when Perspex was used. The inner diameter of the glass cylinder was equal to 75.00 ± 0.02 mm. The width of each straight side and the perpendicular distance between them were both equal to 75.00 ± 0.05 mm. Thus the cross-sectional length-to-breadth ratio was equal to 2.00. Two different right-

circular inner cylinders were used, again machined out of brass. The diameters were equal to 60.00 ± 0.01 and 61.80 ± 0.01 mm. The base and cover of this flow rig were made from aluminium, and each contained a PTFE bearing to support the inner cylinder. The flow region was bounded vertically by two PVC collars. One rested on the base of the flow rig, while the other was connected by metal rods to a micrometer screw assembly. In this way, the height of the flow domain could be varied between zero and 115 mm. Surrounding the two cylinders was a water jacket with plane Perspex walls, through which thermally regulated distilled water was pumped at 27.3°C. This had the effect of holding the temperature, and therefore also the viscosity, of the working fluid constant throughout the course of the experiments. As a further precaution, the entire flow rig was housed in a cabinet in which the air temperature was held at 27°C. For this rig, the working fluid was a 2:1 mixture of glycerol and distilled water, with a kinematic viscosity $\nu = 13.57$ mm^{2}s^{-1} at 27.3°C.

The third rig was the same as the precision one described above in all aspects except the inner cylinder and the end-plates. In this case, the inner cylinder was machined from brass to have a 7.4° linear taper along a length of 100.0 mm. The diameter at the base was equal to 58.0 mm, while at the top it was equal to 32.0 mm. The horizontal end-plates were again made out of PTFE, but were cut in such a way that one fitted around the base of the inner cylinder while the other fitted at the top. This prevented any change in the positions of the end collars, which were held at a fixed vertical separation of 100.0 mm. The working fluid in this case was a 1:1 mixture of distilled water and glycerol, with $\nu = 6.55$ mm^{2}s^{-1} at 27.3°C.

The driving mechanism for each of the three stadium rigs described above consisted of a stepping motor which was connected to the inner cylinder via a 6:1 reduction gearbox and a pulley system. The angular velocity of the inner cylinder was directly proportional to the frequency of the driving signal which was supplied to the stepping motor. This frequency was stable to better than 0.1% over the course of the experiments.

3.2. *Dimensionless parameters*

There are three dimensionless parameters which describe the systems with right-circular inner cylinders. The Reynolds number Re is defined as $Re = \omega r d/\nu$, where ω is the angular speed of the inner cylinder, r is the radius of that cylinder, d is the minimum gap between the inner and outer cylinders and ν is the kinematic viscosity of the working fluid. Also, there is the aspect ratio Γ which is defined as $\Gamma = h/d$, where h is the height of the flow domain. Finally, there is a parameter η which is defined as the ratio of the inner cylinder diameter to the perpendicular distance between the straight sides of the outer stadium. Thus η is the equivalent of the radius ratio parameter which is used in describing the standard Taylor–Couette system. A value of $\eta = 0.824$ was used for the majority of experiments involving the two right-circular stadium systems. However, some experiments were done with $\eta = 0.800$ in the second system.

For the system with the tapered inner cylinder, we define the Reynolds number as $Re = \omega r_{max} d_{min}/\nu$, where once again ω is the angular speed of the inner cylinder, but now r_{max} is the maximum radius along the length of the tapered cylinder, and d_{min} is the absolute minimum gap between the inner cylinder and the stadium. The choice of r_{max}, and consequently d_{min}, was motivated by experimental observations showing that features in the flow field are driven predominantly by the larger radius (see §5). Here, we have $r_{max} = 29.0$ mm and $d_{min} = 8.5$ mm.

3.3. *Data acquisition and analysis*

A laser-Doppler velocimeter (LDV) was used to obtain quantitative information about the flow dynamics. The system is the same one described by Kobine & Mullin (1994), where full details can be obtained. The LDV operated in such a way as to give a continuous output voltage that was directly proportional to the radial velocity component at a chosen point in the flow (see §3.4 below). The resulting velocity time-series were analysed using various signal-processing techniques. Principal among these was the technique of phase-portrait reconstruction based on singular-value decomposition (SVD) as developed by Broomhead & King (1986).

3.4. *Location of measuring points*

An important consideration is the position within the flow at which point measurements should be made. The results from §2 for the two-dimensional flow field prove essential in this respect. If time-series are obtained at a measuring point located in the middle of either the main rotating flow or one of the recirculations then they are found not to be representative of the dynamics as a whole. However, if the measuring point is positioned at the interface between the two regions, then the signal is found to capture the respective time-dependent motions without undue bias to one or the other.

In order to specify our measuring positions in a way which is reproducible, we define three dimensionless Cartesian coordinates x, y and z. The coordinates $x \in [-1, 1]$ and $y \in [-1, 1]$ are measured along the major and minor axes of the stadium respectively, with $(x, y) = (0, 0)$ corresponding to the axis of rotation of the inner cylinder. The third coordinate z is taken in the axial direction, with $z = 0$ corresponding to the bottom end-plate (the location of r_{max} in the case of the tapered inner cylinder) and $z = 1$ corresponding to the top end-plate.

All the measurements which are reported in this paper were made at points located at $x = 0.5 \pm 0.05$, $y = 0.0 \pm 0.1$. This is where the interface between the the main flow and the recirculation is expected on the basis of the numerical results in §2. In the case of the experiments with right-circular inner cylinders, the axial coordinate was fixed at $z = 0.5$ with an accuracy of approximately 1%. Most of the measurements made with the tapered inner cylinder involved a continuous traverse of the measuring point from $z = 0$ to $z = 1$. However, for the cases where the measuring point was fixed, the axial coordinate was $z = 0.15$, again accurate to 1%.

4. Experimental results: right-circular inner cylinder

4.1. *Survey of parameter space*

A series of experiments was carried out using the first stadium apparatus which was described in §3.1. The LDV was used to observe the time-dependent behaviour of the flow over a range of aspect ratio from $\Gamma = 3$ to 11 for $\eta = 0.824$. For these experiments, a background air-conditioning system was used to control the temperature of the working fluid. The temperature was monitored continuously and was found to vary gradually between 21.0 and 22.0°C over the course of the experiments, resulting in a variation in viscosity between 16.9 and 16.7 mm^2s^{-1}. Measurements of the speed of the inner cylinder were always accompanied by measurements of the fluid temperature in order to allow the viscosity, and therefore the Reynolds number, to be determined reasonably accurately (approximately 2%) for the purpose of this initial series of experiments.

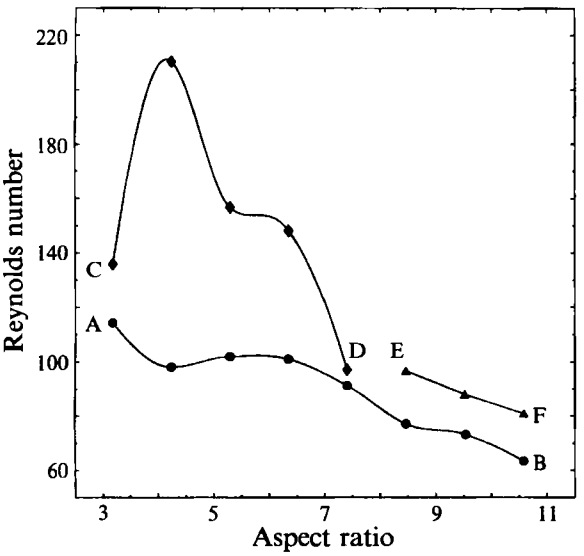

FIGURE 3. Parameter-space diagram showing loci of transitions in right-circular system with $\eta = 0.824$. AB is Hopf bifurcation to singly periodic flow. CD is period-doubling bifurcation. EF is reversible transition between regular and irregular behaviour.

The main bifurcation set which was obtained using the above set-up is shown in figure 3 in the form of a parameter-space diagram whose axes are aspect ratio and Reynolds number. Measurements were made at fixed aspect ratio by carefully varying the Reynolds number. The initial transition from steady to time-dependent flow is marked by the locus AB in figure 3. Hopf bifurcations to singly periodic motion were found at the marked positions along this line. We define the dimensionless frequency Ω of the oscillation as $\Omega = 2\pi f/\omega_c$, where f is the frequency of the oscillation, and ω_c is the angular frequency of the inner cylinder. Values of $\Omega \approx 0.1$ were obtained at the onset of oscillation across the whole range of aspect ratio which was investigated.

The Reynolds number was then increased further to investigate the nonlinear development of this initial oscillation. For aspect ratios between $\Gamma = 3$ and 7.5, the next qualitative change in the motion was that of a period-doubling bifurcation. An example of this transition was recorded at $\Gamma = 5.0$ and is shown in figure 4. The phase portrait shown in figure 4(*a*) was reconstructed from time-series data taken at $(x, y, z) = (0.5, 0, 0.5)$ when the Reynolds number was just below the critical value for period-doubling. The result is a singly periodic limit cycle. The distortion of the limit cycle is due to the presence of harmonics in the signal arising from nonlinear effects which result from placing the measuring volume at the interface between the rotating flow and the recirculating flow.

The Reynolds number was then increased to just beyond the period-doubling bifurcation, resulting in a period-2 limit cycle in phase space as shown in figure 4(*b*). It was also possible to observe the next period-doubling bifurcation from the period-2 oscillation to one where the period was four times that of the original mode. However, the system could not be held in this period-4 window indefinitely because of the drift in Reynolds number due to small changes in the temperature of the fluid.

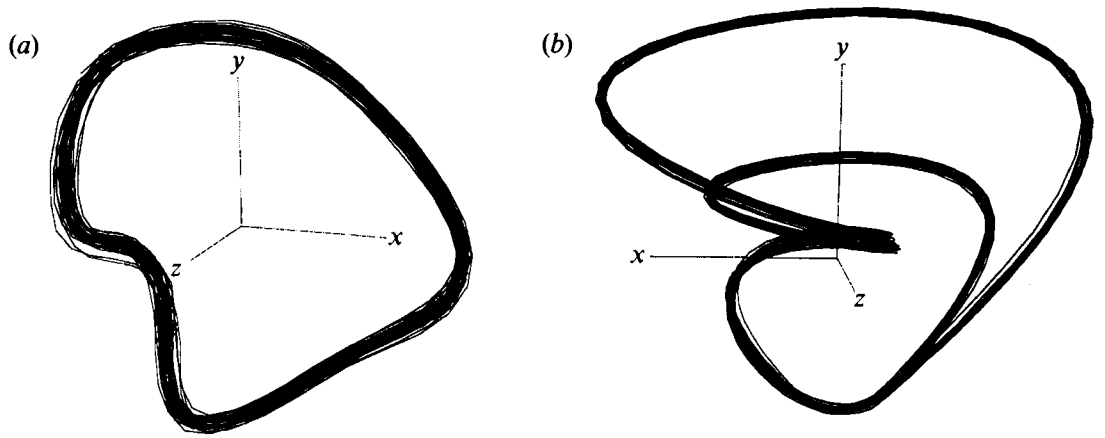

FIGURE 4. Phase portraits showing period-doubling phenomenon in right-circular cylinder at $\Gamma = 5.0$: (*a*) period-1 limit cycle at $Re = 168.5$; (*b*) period-2 limit cycle at $Re = 175.2$. Both attractors sampled at 40 times the fundamental frequency and reconstructed using an embedding dimension $d_E = 20$.

Nevertheless, it proved possible to make relatively accurate measurements ($\sim 2\%$) of the critical Reynolds number for the first period-doubling bifurcation, and this was done for several aspect ratios across the range in question. The results are shown in figure 3 as the locus CD. The general trend with increasing aspect ratio is for the critical Reynolds number for period-doubling (CD) to approach that for the Hopf bifurcation (AB). Indeed, for this set-up with $\eta = 0.824$, it proved impossible to observe a period-doubling bifurcation for aspect ratios greater than that associated with point D in figure 3. This suggests that there is a critical aspect ratio at which the Hopf and the period-doubling events coalesce.

The behaviour which has been described so far can be fully understood in the context of low-dimensional dynamical systems. However, observations were also made of dynamics at higher aspect ratios which do not appear to fall into one of the standard low-dimensional categories. The locus EF in figure 3 consists of points at which there was a sudden but reversible transition between regular oscillatory behaviour and a type of motion which was highly irregular. An example of this transition is shown in figure 5 for $\Gamma = 10.6$. The motion at $Re = 75.6$ consisted of a regular oscillation as represented by the reconstructed phase portrait in figure 5(*a*). The dimensionless frequency of the oscillation in the flow had increased continuously from $\Omega = 0.1$ at onset to $\Omega = 0.2$ at the parameter values of figure 5(*a*).

When the Reynolds number was increased further to $Re = 81.7$, the dynamical behaviour changed qualitatively to the type represented by the phase portrait shown in figure 5(*b*). Colour is used here to indicate the speed of the motion along the trajectories in phase space, where red indicates the slowest motion. Thus it can be see that the dynamics in phase space consist of relatively stationary behaviour (red) punctuated irregularly by large-scale low-frequency excursions (green). The average time scale of these excursions is approximately fifty times the rotation period of the inner cylinder.

The Reynolds number was varied carefully between the two values which are quoted above, and the flow was observed to alter between the two types of behaviour without any evidence of hysteresis. There was also no indication of an intermediate sequence of transitions connecting the two qualitatively distinct types of dynamics.

Furthermore, phase portraits such as the one shown in figure 5(*b*) which were reconstructed from the irregular dynamical behaviour show no obvious low-dimensional structure, at least when represented in a three-dimensional phase space. It certainly did not prove possible to categorize the behaviour as a sequence of well-defined temporal structures separated by quiescent phases, where ideas of intermittency (Pomeau & Manneville 1980) could be applied. Finally, even if the dynamics are contained in a slightly higher-dimensional phase space, it remains the case that they originate directly from singly periodic behaviour. Such a transition does not form part of the established framework of finite-dimensional dynamical systems theory.

4.2. *Robustness of experimental results*

The results described above are, to the best of our knowledge, the first to have been obtained from a stadium-shaped Taylor–Couette system. They were gathered in experiments carried out on a reasonably accurate apparatus, but it could be argued that the observed behaviour may be highly susceptible to small inaccuracies particularly in the narrow region formed by the inner cylinder and the plane walls. Therefore, we considered it necessary to test the robustness of the observed dynamical motion by turning to the second flow rig described in §3. The new apparatus was made to a greater geometrical precision than the first version as all lengths were improved in accuracy by an order of magnitude. In addition, we incorporated a means of controlling the temperature of the working fluid, thereby allowing stricter control of the Reynolds number. The parameter η was set initially to $\eta = 0.824$ as before.

Irregular behaviour was observed once again at moderately large aspect ratios, but to a lesser degree than was the case in the previous system. An example of the motion in question is shown in figure 6 for the aspect ratio $\Gamma = 10.5$. The Reynolds number was increased slowly from zero until the first appearance of a regular oscillation at the Hopf bifurcation. The Reynolds number was then increased to $Re = 90.1$, where the phase-space dynamics changed to the form shown in figure 6. As before, there was the irregular occurrence of low-frequency structures (green), along with sections of approximately steady behaviour (red). The time scale of an individual excursion was approximately fifty times the period of the inner cylinder, which is the value that was recorded for similar features in the first system. However, the average extent of the quiescent phases is now markedly reduced.

The form of the phase portrait in figure 6 could certainly support the interpretation that the system is close to homoclinicity. The passage of trajectories near an unstable fixed point in phase space is liable to give the slowing down and divergence which are indicated by the sections coloured red in figure 6. However, a characteristic feature of the approach to homoclinicity in a dynamical system is always the continuous decrease of mode frequency with variation of the bifurcation parameter. This is not observed in this particular case. Indeed, as was noted previously, the frequency of oscillation actually *increases* as the Reynolds number is increased towards the point where the dynamics undergo qualitative change. It remains the case that there is an apparently sudden and reversible alteration in dynamical characteristics of a type not accounted for by conventional dynamical-systems methods.

Whatever the underlying process, it is seems likely that the stronger irregularity observed in the first of the two systems with right-circular inner cylinders is the result of a combination of small experimental imperfections. The divergence of trajectories seen in figure 6 as the motion in phase space slows down creates a region

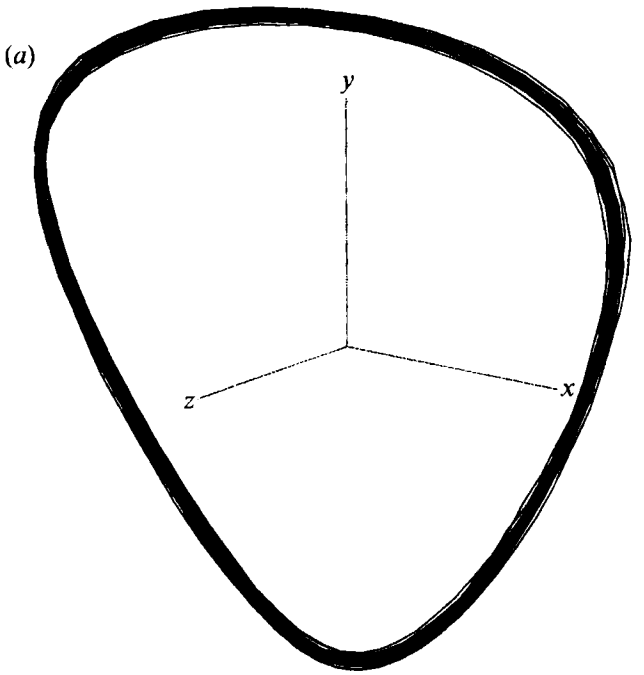

FIGURE 5(a). For caption see facing page.

for amplification of any external irregularities which are introduced into the system. Mechanisms such as this have been studied in detail by Stone & Holmes (1991).

All the observations which have been reported up to this point were obtained for $\eta = 0.824$. However, measurements were also made in the precision apparatus with a different right-circular inner cylinder which gave $\eta = 0.800$. In particular, attention focused on the range of aspect ratio where the apparent change from finite-dimensional behaviour to non-standard behaviour had been observed previously. Results for $\eta = 0.800$ are shown in figure 7 as a parameter-space diagram. Once again, the sequence of Hopf bifurcation followed by period-doubling bifurcation was recorded. However, it proved impossible to reproduce the transition to any form of irregular behaviour at higher aspect ratios similar to that found in the previous systems. A possible reason for this absence can be found in the variation of the loci of Hopf (GH) and period-doubling (JK) bifurcations in figure 7. As was seen in figure 3, the irregular behaviour occurred for aspect ratios above an apparent coalescence of the two bifurcations. The loci of bifurcations shown in figure 7 approach each other initially, but then diverge with further increase of aspect ratio.

Thus it would appear that the flow dynamics are strongly dependent on the value of η. A small change in η between the two systems either prevents the simultaneous occurrence of a Hopf and a period-doubling event, or at least removes it to an aspect ratio which is outside the accessible experimental range. Either way, the existence of the irregular behaviour seems to be related, in a sense as yet undetermined, to the interaction between these two bifurcations. In addition, the fact that a small change (3%) in a geometrical parameter has such a large effect on the dynamics is taken as justification for building the second apparatus to a much greater precision.

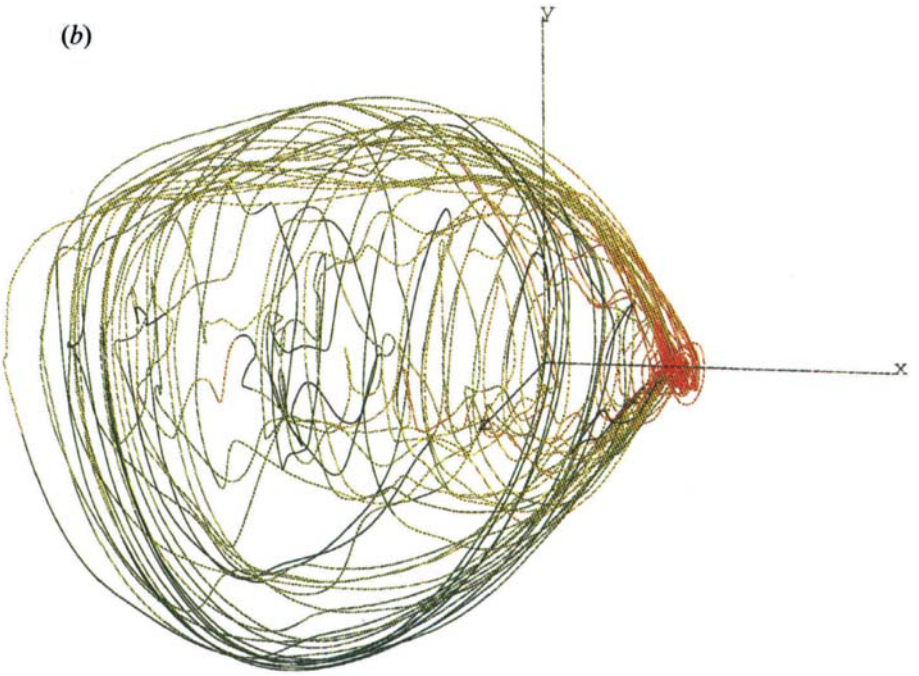

FIGURE 5. Phase portraits showing transition to irregular behaviour at $\Gamma = 10.6$: (*a*) singly periodic oscillation ($Re = 75.6$), sampled at 50 times fundamental frequency, $d_E = 25$; (*b*) irregular behaviour ($Re = 81.7$), $d_E = 200$.

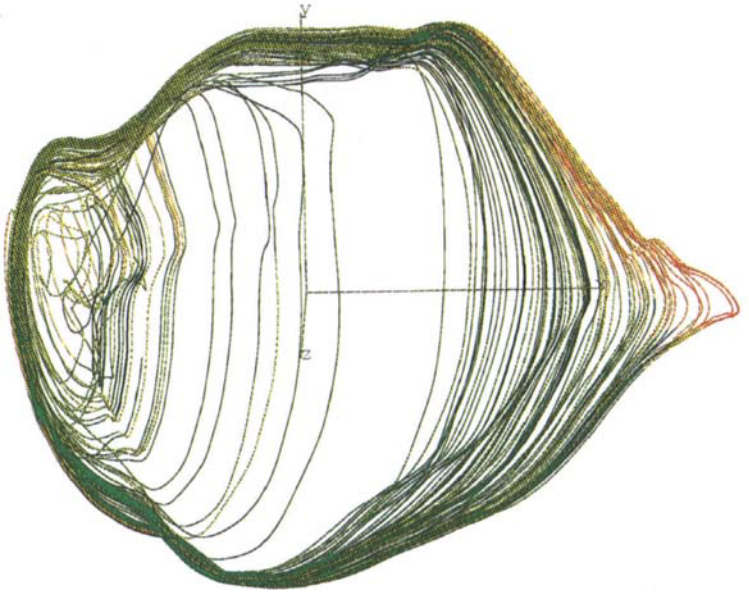

FIGURE 6. Phase portrait showing irregular behaviour in right-circular system with $\eta = 0.824$ at $\Gamma = 10.5$, $Re = 90.1$. $d_E = 160$.

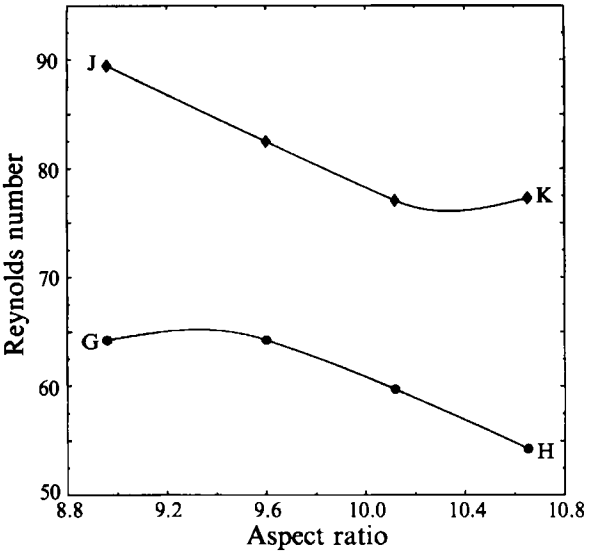

FIGURE 7. Parameter-space diagram showing loci of transitions in right-circular system with $\eta = 0.800$. GH is Hopf bifurcation to singly periodic flow. JK is period-doubling bifucation.

4.3. *Comparison with other fluid systems*

The observation of period-doubling bifurcations in the stadium over a relatively wide range of aspect ratio is at odds with the vast majority of occurrences of period-doubling in fluid systems, which are generally restricted to flows of very limited spatial extent. Examples include the measurements reported by Libchaber & Maurer (1980) of period-doubling in the convection of liquid helium in a small cell where only two convective rolls existed. There is also the first observation of period-doubling in Taylor–Couette flow by Pfister (1985), who studied single-cell flow at aspect ratios much less than one.

Irregular behaviour similar to that described above was observed by Sullivan & Ahlers (1988) in a fluid convection experiment. A binary fluid mixture was contained in a long rectangular box with a temperature difference between the top and bottom surfaces. The system was governed by two dimensionless parameters, namely the Rayleigh number Ra and a separation ratio Ψ which determined whether concentration gradients helped or hindered convection. Over a certain range of the parameter Ψ, it was observed that the first time-dependent flow to appear with gradual increase of Ra consisted of slow bursts which were separated by irregular intervals that were long on the scale of the vertical thermal diffusion time. The transition was found to be reversible, with no evidence of hysteresis. At other values of Ψ, however, the onset of time-dependence was observed by Sullivan & Ahlers to take place via a Hopf bifurcation to a regular singly periodic mode.

An experimental study by Mullin (1993*b*) of flows in a triply connected Taylor–Couette system revealed the existence of both low-dimensional behaviour and a non-standard transition to irregular motion at one particular aspect ratio. The configuration in question consisted of two rotating cylinders placed symmetrically inside a larger stationary circular cylinder. Flow was driven by counter-rotation of the inner cylinders at equal speeds, and there was a movable top-plate which defined the height of the domain. In this way, the system was governed by a Reynolds

number and an aspect ratio, and could be treated in a similar manner to other two-parameter systems. The flow was considered at an aspect ratio of $\Gamma = 3.675$ (based on the minimum distance between an inner cylinder and the outer container) both for quasi-static increases of the Reynolds number from zero and for sudden increases. It was observed that the onset of time-dependence in the continuously evolved mode occurred as the result of a Hopf bifurcation to a singly periodic state, and that further increase of Re resulted in the appearance of a quasi-periodic mode followed by the onset of weakly chaotic behaviour. Such a sequence has been observed in a variety of fluid systems, and is consistent with the finite-dimensional route to chaos proposed by Ruelle & Takens (1971).

In addition, a steady disconnected mode was located by Mullin in which very different dynamics were found to develop. A Hopf bifurcation to singly periodic flow was again detected, but this time with much smaller amplitude. On increasing the Reynolds number, occasional large-amplitude bursts were observed to occur within the otherwise regular oscillation. The average separation between these intermittent features decreased as Re was increased. The behaviour was reminiscent of the type-I intermittent route to chaos proposed by Pomeau & Manneville (1980). Indeed, it was found that the average period of recurrence in the triply-connected Taylor–Couette flow close to the first appearance of the bursts scaled in the same way as that predicted by Pomeau & Manneville. However, the theory also predicts that there should be a low-frequency cut-off in the distribution. This was not observed by Mullin, and it was concluded that this transition to chaos was not governed by one of the known finite-dimensional mechanisms.

5. Experimental results: tapered inner cylinder

We now turn to the case where the rotating inner cylinder is tapered as opposed to right circular. The approach was to increase the Reynolds number gradually at constant aspect ratio and categorize the different types of flow behaviour which were observed. The results of this process are set out below.

5.1. *Steady flow*

For Reynolds numbers up to 89.4, the flow was observed to be steady. Vertical profiles of radial velocity revealed a steady 'two-cell' flow structure, where the cells were of unequal size. A typical radial velocity profile for this steady flow is shown in figure 8(a) for $Re = 75.7$. All such profiles in this study were obtained by traversing the measuring point along the line $(x, y) = (0.5, 0)$ (see §3.4) from the botton end-plate to the top at a constant speed of 0.1 mm s^{-1}. The radial velocity component was sampled at a rate of 1 Hz during the traverse. Profiles appear skewed with respect to the zero velocity line due to the limited precision with which the LDV measuring point could be positioned on the major axis of the stadium ($y = 0$).

The profile shown in figure 8(a) indicates that all the significant secondary flow is strongly compressed towards the end where the gap between the inner and outer cylinders is narrowest. Close to the bottom collar, the radial flow component is directed inward towards the rotating cylinder. As the height of the measuring position is increased, the radial flow changes to having the form of an outwardly directed jet. With further increase of height, the profile shows there to be a change back to weak inward flow over a broad region. Thus there is a small cell being driven strongly at the bottom end, with a much larger and weaker cell above it.

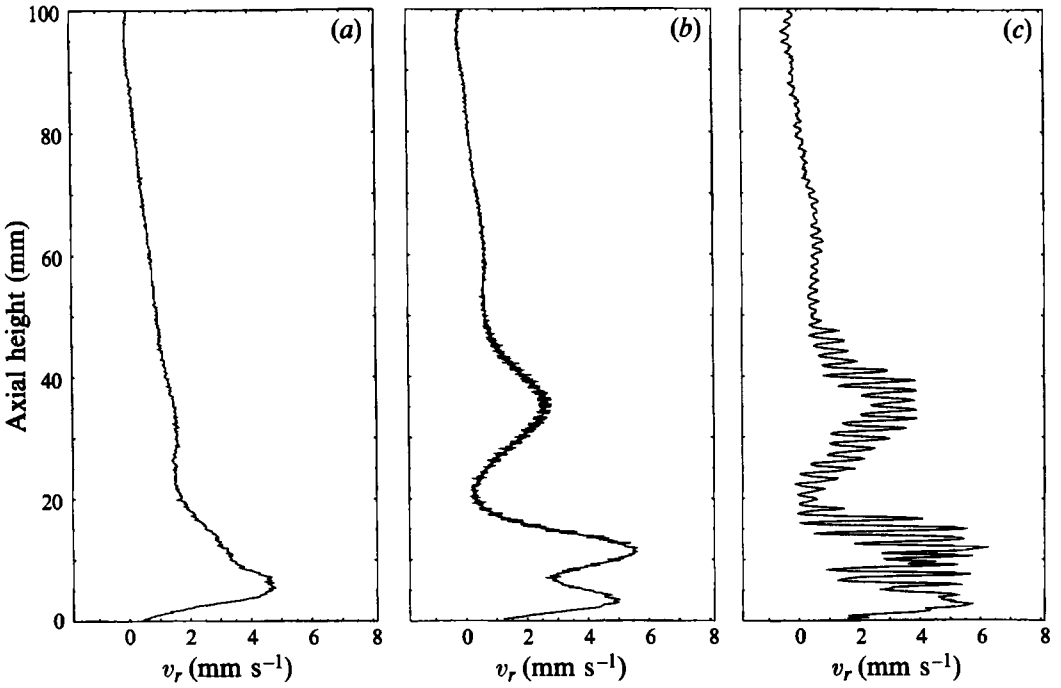

FIGURE 8. Typical radial velocity profiles for flow in tapered system: (*a*) steady flow at $Re = 75.7$; (*b*) singly periodic flow at $Re = 101.0$; (*c*) quasi-periodic flow at $Re = 113.6$.

5.2. *Singly periodic flow*

The next range of Reynolds number which was identified experimentally was between $Re = 89.4$ and 109.5. In this range, the flow was observed to be singly periodic with a dimensionless frequency $\Omega = 0.087$. A typical radial velocity profile, taken at $Re = 101.0$, is shown in figure 8(*b*). The traverse conditions were the same as those used to obtain figure 8(*a*). Figure 8(*b*) and others like it are not time-series as such, but show rather the overall variation of oscillation amplitude with axial position in the flow. The profile in figure 8(*b*) reveals that there is now a second vortex pair above the one which was identified at smaller vales of *Re*. This second pair was found to grow continuously as *Re* was increased.

5.3. *Quasi-periodic and chaotic flow*

For $Re = 109.5$ to 123.2, the oscillatory motion in the flow was found to be quasi-periodic, with the second dimensionless frequency equal to 0.012. A typical profile was recorded at $Re = 113.6$ and is shown in figure 8(*c*). The cellular state here is basically the same as that for $Re = 101.0$. However, the quasi-periodic temporal motion is not obvious from the spatial profile. Instead, velocity time-series were recorded from a fixed position in the flow domain. In these experiments, the measuring position was fixed at $(x, y, z) = (0.5, 0, 0.15)$. This position corresponded approximately to the maximum spatial amplitude of the oscillation. The velocity time-series were used to reconstruct phase-space representations of the dynamics using the methods proposed by Broomhead & King (1986). Visualization of the phase portraits obtained in this way was achieved by means of Poincaré sections through the full set of

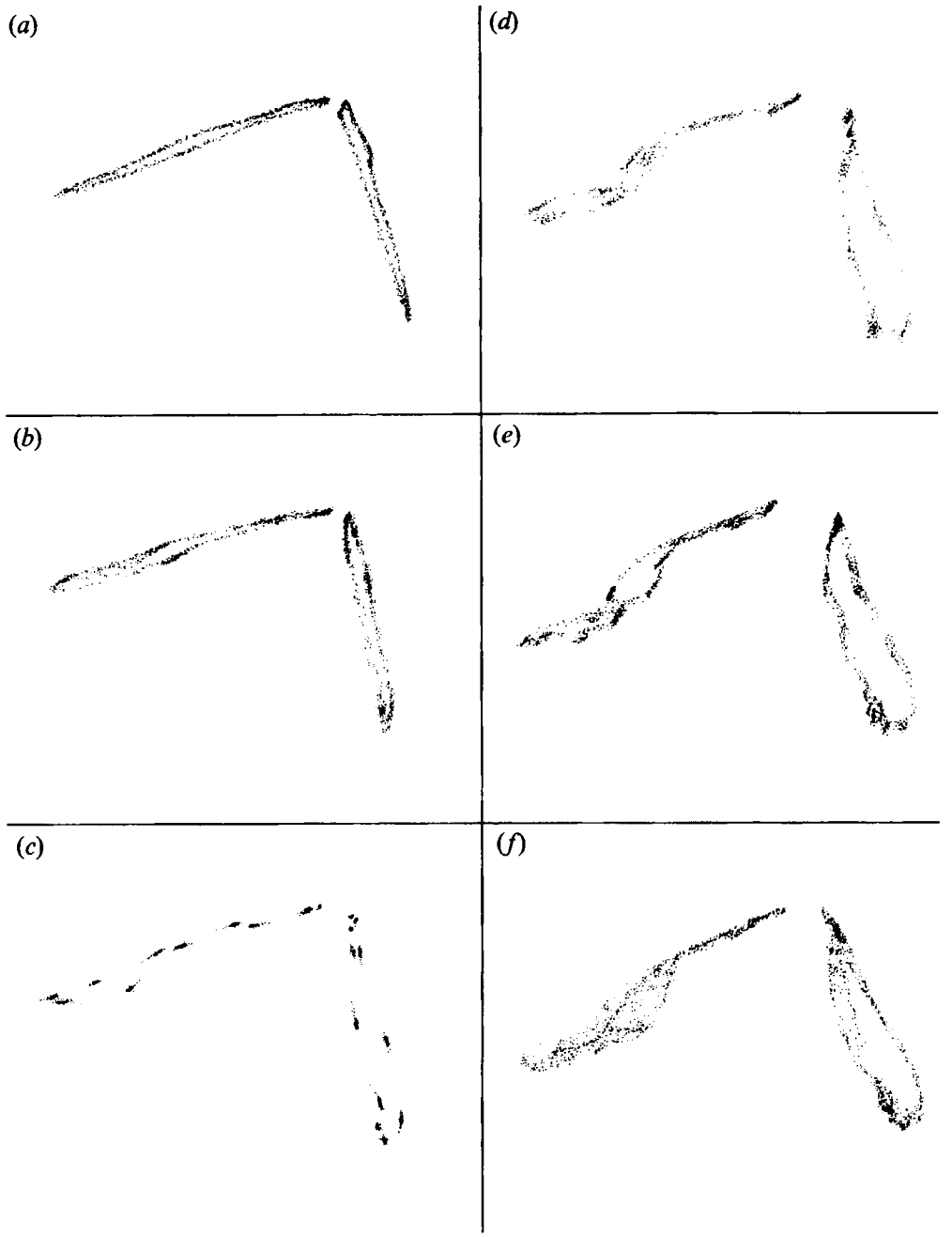

FIGURE 9. Poincaré sections through reconstructed phase portraits for tapered system: (*a*) $Re = 118.2$; (*b*) $Re = 120.9$; (*c*) $Re = 123.2$; (*d*) $Re = 124.2$; (*e*) $Re = 124.6$. All attractors sampled at 50 times the primary frequency with embedding dimension $d_E = 100$.

trajectories. The results are shown in figure 9(*a–f*) for successively larger values of *Re*.

The Poincaré section shown in figure 9(*a*) corresponds to $Re = 118.2$. The presence of two loops indicates a torus in phase space, and the fact that the loops are closed

implies that the frequencies of the two dynamic modes are incommensurate. On increasing the Reynolds number to $Re = 120.9$, the distribution of points in the plane of section, as shown in figure 9(*b*), becomes non-uniform suggesting the onset of frequency locking. The torus becomes fully locked with a frequency ratio of 11:2 when the Reynolds number is increased to $Re = 123.2$, as shown in figure 9(*c*).

Thus far, the observed dynamics in the tapered system were all regular. However, it was found that a chaotic regime is entered when the Reynolds number is increased from the locked state which was shown in figure 9(*c*). The sequence of Poincaré sections in figure 9(*d–f*) corresponds to $Re = 123.6$, 124.2 and 124.6 respectively. These show the structure of the phase-space torus becoming progressively more irregular, indicating the development of chaotic dynamics within the flow. However, the chaos is not without structure, as can be seen from the persistence of the two distinct loops in the Poincaré section.

5.4. *Non-standard irregular behaviour*

The next qualitative change in the dynamics occurred at $Re = 128.1$. When the Reynolds number was increased to this value, the flow was observed to jump from the chaotic state to a regular singly periodic mode. The dimensionless frequency of the new oscillation was measured as $\Omega = 0.063$ independent of Reynolds number over the parameter range in which it was observed. On decreasing the Reynolds number, the flow did not revert back to the chaotic state until $Re = 122.3$. There was therefore hysteresis between these two types of behaviour. This can be seen from the two velocity profiles in figure 10, both of which were recorded at $Re = 126.2$. In figure 10(*a*), the flow is chaotic, whereas in figure 10(*b*) the flow is singly periodic and regular.

The final stage of the investigation was to increase the Reynolds number further and determine the evolution of the singly periodic mode which appears abruptly at $Re = 128.1$. When this was done, it was found that the dynamics develop continuously from regular at $Re = 128.1$ to highly irregular at $Re = 157.7$. There is no evidence of a sequence of discrete transitions leading to this disordered state. A typical time-series of the irregular behaviour was recorded at $Re = 152.7$, and is shown in figure 11. The continuous nature of the transformation can be seen from the sequence of phase portraits in figure 12(*a–c*). Discrete points are plotted at equal time intervals along the trajectories. Lines linking successive points are not shown now for the sake of clarity. In figure 12(*a*), the outline of the original limit cycle is still discernible. This becomes less so in figure 12(*b*), until finally in figure 12(*c*) there is very little obvious structure.

5.5. *Estimates of correlation dimension*

Thus we have observed the devlopment of two types of irregular behaviour in the tapered stadium system. The first was the result of frequency locking of a phase-space torus which then broke down to apparently chaotic motion. The second type involved the continuous development of dynamics with no obvious low-dimensional characteristics. In order to emphasize this difference, we have applied some standard techniques to estimate the correlation dimension of the two types of behaviour. The methods used were the same as those developed by Buzug & Pfister (1992)

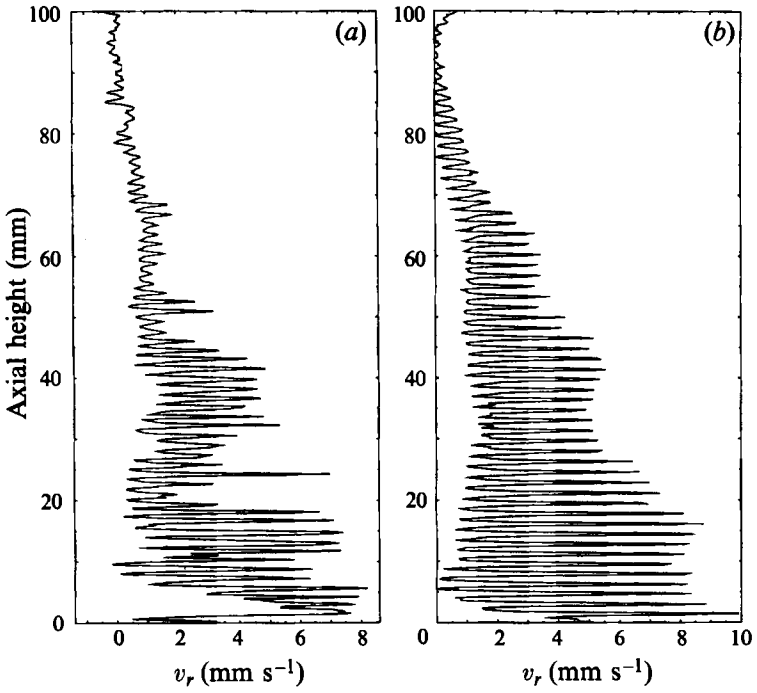

FIGURE 10. Radial velocity profiles at $Re = 126.2$ showing hysteresis in tapered system: (*a*) chaotic mode; (*b*) regular singly periodic mode.

and Buzug, Stamm & Pfister (1993), which are based on the Grassberger–Procaccia method but with improvements to reduce the adverse effects of finite data size and experimental noise. Correlation dimensions were calculated as a function of embedding dimension, whereby any genuine low-dimensional behaviour gives rise to a staturation of correlation dimension for sufficiently large embedding dimension.

For the case of the first sequence of transitions (illustrated in figure 9), the saturated correlation dimension D_2 was calculated at various Reynolds numbers from 120 to 143. Beginning at $Re = 120$, a value of $D_2 \approx 2.0 \pm 0.1$ was obtained which is consistent with the observed phase-space torus (figure 9*a*). There was a local minimum of $D_2 \approx 1.5 \pm 0.1$ at $Re = 123$, corresponding to the stage at which the torus becomes fully locked (figure 9*c*). As the torus broke up, the correlation dimension rose to $D_2 \approx 2.4 \pm 0.2$ at $Re = 126$ and remained at this value up to the maximum measured Reynolds number of 143.

However, for the second type of behaviour, there was no observed saturation of correlation dimension with embedding dimension. The dimension of the dynamics illustrated in figure 12(*c*) was calculated over a range of embedding dimensions, with $D_2 \approx 3$ at $d_E = 4$ rising to $D_2 \approx 6$ at $d_E = 12$. Beyond this point, any calculated dimension is meaningless due to the finite length of the time-series being analysed.

Finally, it is interesting to note that the primary oscillatory mode, whose actual frequency is 0.066 Hz, develops low-dimensional chaos with increasing Re, while the secondary singly periodic mode with a frequency of 0.063 Hz evolves to a state with no discernible structure. Such different outcomes from an initial quantitative difference of less than 5% suggests that some characteristic feature of the geometry may be involved in controlling the dynamics.

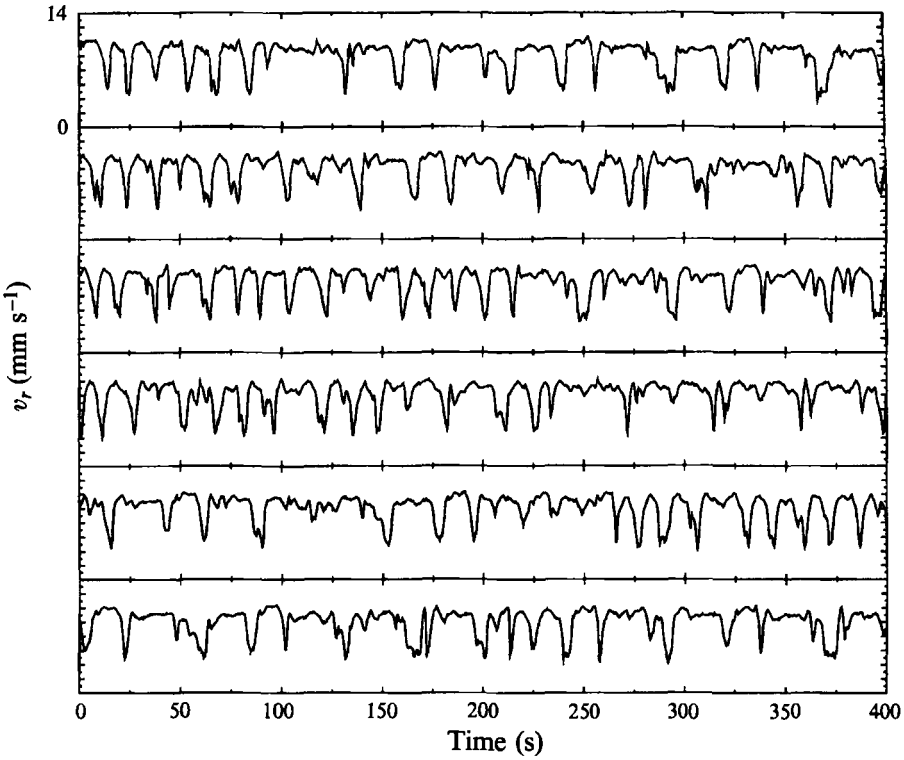

FIGURE 11. Example of irregular behaviour that develops smoothly from the secondary singly periodic mode in the tapered system. Time series of radial velocity component measured at $(x, y, z) = (0.5, 0, 0.15)$ over 2400 s. $Re = 152.7$. The right-hand edge of each strip connects to the left-hand edge of the one above.

6. Conclusions

Understanding the origins of turbulence in fluid flow still presents a fundamental challenge despite more than a century of research. Recently, the field of finite-dimensional dynamical systems has allowed some progress to be made towards this goal. A notable example is Taylor–Couette flow, where ideas from dynamical systems have resulted in significant advancements beyond the level of weakly nonlinear stability theory.

In this paper, we have presented experimental results which show that finite-dimensional behaviour persists in versions of the Taylor–Couette problem with discrete Z_2 azimuthal symmetry. Although new flow phenomena were observed, many of the finite-dimensional mechanisms associated with the original Taylor–Couette system were reproduced in the stadium variants. It is considered significant that this was the case even in the absence of travelling waves, which are prohibited by symmetry. This fact is taken as further support for the view that low-dimensional dynamics are controlled at a fundamental level by codimension-2 points in the parameter space of the problem. Such points are only possible in a physical system with finite vertical extent. They do not occur in the periodic model of Taylor–Couette flow, which supports travelling waves but none of the complicated dynamics which are observed experimentally.

Nevertheless, the question remains as to whether all driven internal flows necessarily

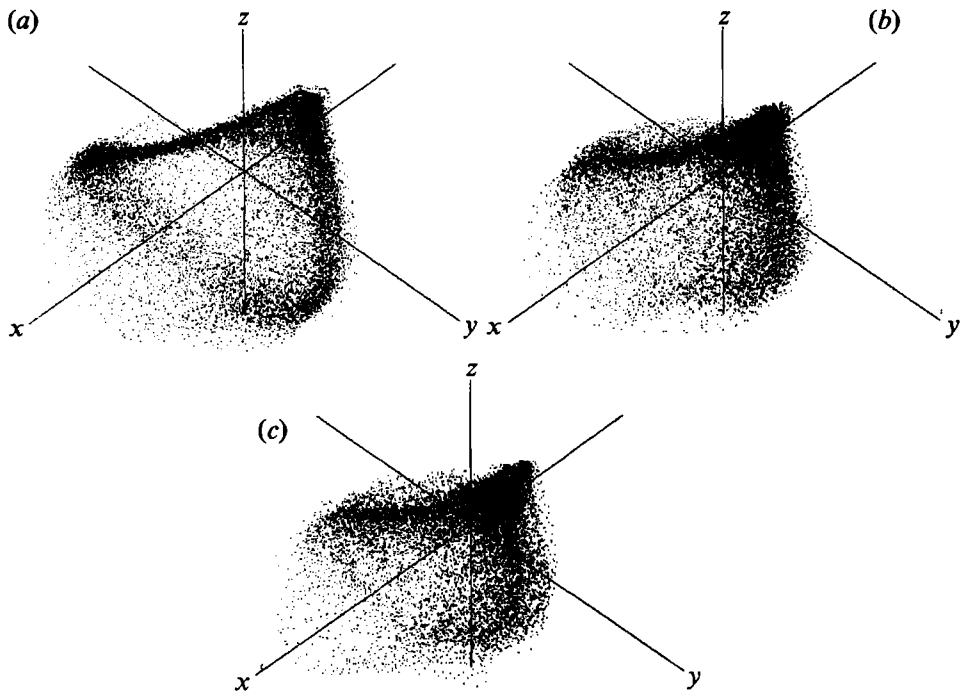

FIGURE 12. Phase portraits showing continuous transformation of secondary singly periodic mode: (*a*) $Re = 142.8$; (*b*) $Re = 147.7$; (*c*) $Re = 152.7$. Sampled at 3 Hz $d_E = 20$.

give rise to bifurcations. The present study has extended the range of flows for which this is the case. However, behaviour of a type other than finite-dimensional was observed at moderately large aspect ratio with the tapered inner cylinder. Such observations, together with those made by Mullin (1993*b*) of flow in a triply connected Taylor–Couette system, suggest that bifurcation phenomena occur in closed flows as a subset of the possible mechanisms for flow transition.

Further experimental evidence has been given which supports the view put forward by Ruelle & Takens (1971) that chaotic flow behaviour can arise after the appearance of only a small number of modes. This is in contrast to the well-known Landau hypothesis, which views turbulence as the sum of an infinite number of modes. Experiments by Gollub & Swinney (1975) on the standard Taylor–Couette problem gave what appeared to be the first evidence of the Ruelle–Takens mechanism operating in a fluid flow. However, Coughlin & Marcus (1992) have argued that a quasi-periodic flow in a system with continuous $SO(2)$ symmetry will appear as only a singly periodic flow from the frame of reference which rotates with the primary wave. They therefore question the validity of the experimental evidence obtained by Gollub & Swinney. Observations of the Ruelle–Takens mechanism are required in fluid systems with more generic symmetries. Some such observations have already been made (Gollub & Benson 1980; Mullin 1993*b*), but clearly more are required before any firm claims can be made.

Finally, the results of this study emphasize again the need for a systematic approach to the investigation of dynamics in fluid flow. Subtle features such as the coalescence of lines of bifurcations or the locking and subsequent break-up of a phase-space torus

prove to be the key to understanding the dynamics as a whole. Only if the greatest of care is exercised can such features be uncovered and resolved.

This work was funded by the SERC (UK) through the Nonlinear Initiative (T. M.) and through a postgraduate studentship (J. J. K.). The support of a European Community Fellowship (ERB4040PL910051) is also acknowledged (T. J. P.). The authors wish to express their sincere thanks to Mr K. Long for his technical expertise in the experimental part of the study.

REFERENCES

BOUROT, J. M. 1969 Sur l'application d'une méthode de moindres carrés à la résolution approchée du problème aux limites, pour certaines catégories d'écoulements. *J. Méc.* **8**, 301–322.

BROOMHEAD, D. S. & KING, G. P. 1986 Extracting qualitative dynamics from experimental data. *Physica* D **20**, 217–236.

BUZUG, TH. & PFISTER, G. 1992 Optimal delay time and embedding dimension for delay-time coordinates by analysis of the global static and local dynamical behaviour of strange attractors. *Phys. Rev.* A **45**, 7073–7084.

BUZUG, TH., STAMM, J. VON & PFISTER, G. 1993 Characterization of period-doubling scenarios in Taylor–Couette flow. *Phys. Rev.* E **47**, 1054–1065.

COUGHLIN, K. T. & MARCUS, P. S. 1992 Modulated waves in Taylor–Couette flow. Part 1. Analysis. *J. Fluid Mech.* **234**, 1–18.

DI PRIMA, R. C. & SWINNEY, H. L. 1981 Instabilities and transition in the flow between concentric rotating cylinders. In *Hydrodynamic Instabilities and the Transition to Turbulence* (ed. H. L. Swinney & J. P. Gollub). Springer.

GOLLUB, J. P. & BENSON, S. H. 1980 Many routes to turbulent convection. *J. Fluid Mech.* **100**, 449–470.

GOLLUB, J. P. & SWINNEY, H. L. 1975 Onset of turbulence in a rotating fluid. *Phys. Rev. Lett.* **35**, 927–930.

HELLOU, M. & COUTANCEAU, M. 1992 Cellular Stokes flow induced by rotation of a cylinder in a closed channel. *J. Fluid Mech.* **236**, 557–577.

KOBINE, J. J. & MULLIN, T. 1994 Low-dimensional bifurcation phenomena in Taylor–Couette flow with discrete azimuthal symmetry. *J. Fluid Mech.* **275**, 379–405.

LIBCHABER, A. & MAURER, J. 1980 Une experience de Rayleigh–Bénard de géométrie réduite; multiplication, accrochage et démultiplication de fréquencies. *J. Phys. Paris* **41**, C3–51.

MOFFATT, H. K. 1964 Viscous and resistive eddies near a sharp corner. *J. Fluid Mech.* **18**, 1–18.

MULLIN, T. 1993*a* Chaos in fluid dynamics. In *The Nature of Chaos* (ed. T. Mullin). Oxford University Press.

MULLIN, T. 1993*b* Disordered fluid motion in a small closed system. *Physica* D **62**, 192–201.

MULLIN, T. & LORENZEN, A. 1985 Bifurcation phenomena in flows between a rotating circular cylinder and a stationary square outer cylinder. *J. Fluid Mech.* **157**, 289–303.

MULLIN, T., LORENZEN, A. & PFISTER, G. 1983 Transition to turbulence in a non-standard rotating flow. *Phys. Lett.* A **96**, 236–238.

MULLIN, T. & PRICE, T. J. 1989 An experimental observation of chaos arising from the interaction of steady and time-dependent flows. *Nature* **340**, 294–296.

PFISTER, G. 1985 Deterministic chaos in rotational Taylor–Couette flow. In *Flow of Real Fluids* (ed. G. E. A. Meier & F. Obermeier). Lecture Notes in Physics, Vol. 235, pp. 199–210. Springer.

POMEAU, Y. & MANNEVILLE, P. 1980 Intermittent transition to turbulence in dissipative dynamical systems. *Commun. Math. Phys.* **74**, 189–197.

PROSNAK, W. J. 1987 *Computation of Fluid Motion in Multiply-connected Domains*, Chap. 6. Braun.

RUELLE, D. & TAKENS, F. 1971 On the nature of turbulence. *Commun. Math. Phys.* **20**, 167–192.

SCHUMACK, M. R., SCHULTZ, W. W. & BOYD, J. P. 1992 Taylor vortices between elliptical cylinders. *Phys. Fluids* A **4**, 2578–2581.

ŠIL'NIKOV, L. P. 1965 A case of the existence of a denumerable set of periodic motions. *Sov. Math. Dokl.* **6**, 163–166.

SMITH, G. P. & TOWNSEND, A. A. 1982 Turbulent Couette flow between concentric cylinders at large Taylor numbers. *J. Fluid Mech.* **123**, 187–217.

SNYDER, H. A. 1968 Experiments on rotating flows between noncircular cylinders. *Phys. Fluids* **11**, 1606–1611.

STONE, E. & HOLMES, P. 1991 Unstable fixed points, heteroclinic cycles and exponential tails in turbulence production. *Phys. Lett.* A **155**, 29–42.

SULLIVAN, T. S. & AHLERS, G. 1988 Nonperiodic time-dependence at the onset of convection in a binary liquid mixture. *Phys. Rev.* A **38**, 3143–3146.

TERADA, T. & HATTORI, K. 1926 Some experiments on the motions of fluids. Part 4. Formation of vortices by rotating disc, sphere or cylinder. *Rep. Tokyo Univ. Aeronaut. Research Inst.* **2**, 287–326.